



Article

Development of the 12-Base Short Dimeric Myogenetic Oligodeoxynucleotide That Induces Myogenic Differentiation

Koji Umezawa ^{1,2,†}, Rena Ikeda ^{3,†}, Taiichi Sakamoto ⁴ , Yuya Enomoto ¹, Yuma Nihashi ⁵ , Sayaka Shinji ³, Takeshi Shimosato ^{1,2,3} , Hiroshi Kagami ¹ and Tomohide Takaya ^{1,2,3,*}

¹ Department of Agricultural and Life Sciences, Faculty of Agriculture, Shinshu University, 8304 Minami-minowa, Kami-ina 399-4598, Japan; koume@shinshu-u.ac.jp (K.U.); 20a1007h@shinshu-u.ac.jp (Y.E.); shimot@shinshu-u.ac.jp (T.S.); kagami@shinshu-u.ac.jp (H.K.)

² Department of Biomolecular Innovation, Institute for Biomedical Sciences, Shinshu University, 8304 Minami-minowa, Kami-ina 399-4598, Japan

³ Department of Agriculture, Graduate School of Science and Technology, Shinshu University, 8304 Minami-minowa, Kami-ina 399-4598, Japan

⁴ Department of Life Science, Faculty of Advanced Engineering, Chiba Institute of Technology, 2-17-1 Tsudanuma, Narashino-shi 275-0016, Japan; taiichi.sakamoto@p.chibakoudai.jp

⁵ Cellular and Molecular Biotechnology Research Institute, National Institute of Advanced Industrial Science and Technology, Central 5-41, 1-1-1 Higashi, Tsukuba 305-8565, Japan; y-nihashi@aist.go.jp

* Correspondence: ttakaya@shinshu-u.ac.jp

† These authors contributed equally to this work.

Abstract: A myogenetic oligodeoxynucleotide (myoDN), iSN04 (5'-AGA TTA GGG TGA GGG TGA-3'), is a single-stranded 18-base telomeric DNA that serves as an anti-nucleolin aptamer and induces myogenic differentiation, which is expected to be a nucleic acid drug for the prevention of disease-associated muscle wasting. To improve the drug efficacy and synthesis cost of myoDN, shortening the sequence while maintaining its structure-based function is a major challenge. Here, we report the novel 12-base non-telomeric myoDN, iMyo01 (5'-TTG GGT GGG GAA-3'), which has comparable myogenic activity to iSN04. iMyo01 as well as iSN04 promoted myotube formation of primary-cultured human myoblasts with upregulation of myogenic gene expression. Both iMyo01 and iSN04 interacted with nucleolin, but iMyo01 did not bind to berberine, the isoquinoline alkaloid that stabilizes iSN04. Nuclear magnetic resonance revealed that iMyo01 forms a G-quadruplex structure despite its short sequence. Native polyacrylamide gel electrophoresis and a computational molecular dynamics simulation indicated that iMyo01 forms a homodimer to generate a G-quadruplex. These results provide new insights into the aptamer truncation technology that preserves aptamer conformation and bioactivity for the development of efficient nucleic acid drugs.

Keywords: aptamer; G-quadruplex; myogenetic oligodeoxynucleotide (myoDN); myogenic differentiation; nuclear magnetic resonance (NMR); nucleolin

Key Contribution: This study reports the structure-based shortening of a myogenetic oligodeoxynucleotide, iSN04, as an anti-nucleolin aptamer that induces myogenesis. The shortening technology of aptamers while maintaining their conformation and activity improves their potency of drug function and synthesis cost.



Citation: Umezawa, K.; Ikeda, R.; Sakamoto, T.; Enomoto, Y.; Nihashi, Y.; Shinji, S.; Shimosato, T.; Kagami, H.; Takaya, T. Development of the 12-Base Short Dimeric Myogenetic Oligodeoxynucleotide That Induces Myogenic Differentiation. *BioTech* **2024**, *13*, 11. <https://doi.org/10.3390/biotech13020011>

Received: 17 March 2024

Revised: 22 April 2024

Accepted: 23 April 2024

Published: 25 April 2024



Copyright: © 2024 by the authors. Licensee MDPI, Basel, Switzerland. This article is an open access article distributed under the terms and conditions of the Creative Commons Attribution (CC BY) license (<https://creativecommons.org/licenses/by/4.0/>).

1. Introduction

Myogenic progenitor cells, called myoblasts, differentiate into myocytes, fuse into multinucleated myotubes, and eventually form myofibers during skeletal muscle development and regeneration. Myogenic differentiation is thus an initial key step for muscle growth and maintenance [1]. However, aging, chronic kidney disease, cancer, or diabetes mellitus decrease the differentiation capacity of myoblasts [2–5], which is one of the reasons

for age- and disease-associated muscle loss such as sarcopenia and cancer cachexia. Therefore, molecules that enhance myogenesis may be promising drugs to prevent the muscle wasting that is increasing in aging societies. Oligodeoxynucleotides (ODNs) have been studied as nucleic acid aptamers that bind to their targets in a conformation-dependent manner with high specificity and affinity, similar to antibodies. Nowadays, aptamers are one of the potential next-generation drugs [6]. We have recently reported a series of myogenetic ODNs (myoDNs), which are single-stranded 18-base telomeric phosphorothioated (PS)-ODNs, that robustly induce myogenic differentiation of myoblasts [7] and rhabdomyosarcoma [8]. The nucleic acids containing telomeric hexamers (5'-TTA GGG-3'), such as myoDNs, are known to form guanine (G)-quartet/quadruplex structures and to recruit DNA/RNA-binding proteins [6]. Indeed, one of the myoDNs, iSN04 (5'-AGA TTA GGG TGA GGG TGA-3'), serves as an aptamer that physically interacts with nucleolin, a multifunctional RNA-binding phosphoprotein localized in myoblast nuclei [7,9]. Antagonizing nucleolin with iSN04 reverses nucleolin-inhibited translation of p53 mRNA and improves p53 protein levels, resulting in enhanced myogenesis [7]. Since iSN04 restores myoblast differentiation deteriorated by diabetes mellitus [10] or cancer-secreted factors [11], it is expected to be a drug seed to reverse muscle loss in these diseases. In addition, nucleolin inhibition by iSN04 suppresses inflammatory responses [12] and induces myocardial differentiation of pluripotent stem cells [13] by modulating the β -catenin signaling pathway. These results suggest that iSN04 may be applicable to inflammatory muscle diseases such as dystrophy and to cardiac regeneration therapy.

iSN04 is incorporated into myoblasts without a carrier [7]. In general, single-stranded PS-ODNs can be spontaneously incorporated into the cytoplasm by an endocytic process termed gymnosis, in part due to their lower molecular weights compared to double-stranded nucleotides [14]. Since shorter PS-ODNs are more favorable for intracellular uptake, sequence shortening is important pharmaceutically to improve drug efficacy and is also beneficial industrially to reduce synthesis costs [15]. In this study, we attempted to shorten iSN04 while maintaining its myogenetic activity. In the previous report, computational simulations and mutational experiments revealed that the guanine stack (G-stack; GGG at the 13–15th bases) within iSN04 is the core structure. Interestingly, an isoquinoline alkaloid, berberine, binds to the G-stack and enhances the activity of iSN04 [7,9]. By forming a complex, berberine is thought to shift the conformation of iSN04 to a more stable and active form, suggesting that the ODNs that configure the G-stack may serve as myoDNs. Here, we investigated the myogenetic activities of the 11–16-base non-telomeric PS-ODNs predicted to form the G-stack structure. Several PS-ODNs successfully induced human, mouse, and chicken myoblast differentiation as well as iSN04 does. These results provide new insights into the design of shorter aptamers.

2. Materials and Methods

2.1. Oligonucleotides

PS-ODNs in which all phosphodiester bonds were phosphorothioated to enhance nuclease resistance in cell culture were synthesized and HPLC-purified (GeneDesign, Osaka, Japan) [7,16]. Unmodified oligonucleotides (DNA and RNA) without phosphorothioate for nuclear magnetic resonance (NMR) and native polyacrylamide gel electrophoresis (PAGE) were synthesized and HPLC-purified (Hokkaido System Science, Sapporo, Japan). The oligonucleotide sequences are listed in Table 1. iMyo01–iMyo08 are the myoDN candidates designed and evaluated in this study. They have two G groups (GGG or GGGG) separated by a mini linker (T or TGA), thymines at the 5' end (TT or TTT), and adenines at the 3' end (AA or AAA). iSN04 is a positive control that induces myogenesis. iSN14 and iSN45 are negative controls that have no myogenic capacity [7]. iMyo01-CS is a reverse complementary strand DNA to iMyo01. In this study, 12nt-Ctrl is a negative control DNA that does not form a G-quadruplex, and 12nt-Ctrl-CS is a reverse complementary strand RNA to 12nt-Ctrl. All oligonucleotides were dissolved in endotoxin-free water, and an equal volume of water without oligonucleotide was used as a control.

Table 1. Oligonucleotide sequences.

Name	Nucleotide	Sequence (5'-3')	Reference
iMyo01	PS-ODN	TTGGGTGGGGAA	This study
iMyo02	PS-ODN	TTTGGGTGGGGAAA	This study
iMyo03	PS-ODN	TTGGGTGAGGGGAA	This study
iMyo04	PS-ODN	TTTGGGTGAGGGGAAA	This study
iMyo05	PS-ODN	TTGGGTGGGAA	This study
iMyo06	PS-ODN	TTTGGGTGGGAAA	This study
iMyo07	PS-ODN	TTGGGTGAGGGAA	This study
iMyo08	PS-ODN	TTTGGGTGAGGGAAA	This study
iSN04	PS-ODN	AGATTAGGGTGAGGGTGA	[7]
iSN14	PS-ODN	ACATTAGGGTGAAAATGA	[7]
iSN45	PS-ODN	GATCCTCAAGCTTAGGTC	[7]
iMyo01-DNA	DNA	TTGGGTGGGGAA	This study
iMyo01-CS	DNA	TTCCCCACCCAA	This study
12nt-Ctrl	DNA	GCATTGGTATTC	[17]
12nt-Ctrl-CS	RNA	GAAUACCAAUGC	This study

2.2. Myoblast Culture

All myoblasts were cultured on the dishes/plates coated with collagen type I-C (Cell-matrix; Nitta Gelatin, Osaka, Japan) at 37 °C under 5% CO₂ throughout the experiments.

The commercially available human myoblast (hMB) stock isolated from a healthy 35-year-old female (CC-2580, lot 0000483427; Lonza, Walkersville, MD, USA) was used [7,10]. hMBs were maintained in Skeletal Muscle Growth Media-2 (CC-3245; Lonza) as a growth medium (GM) for hMB (hGM). For the screening system, 6.0×10^3 hMBs/100 µL hGM/well were seeded on 96-well plates (AS ONE, Osaka, Japan). For high-resolution imaging, 1.0×10^5 hMBs were seeded on 30-mm dishes (AS ONE). For quantitative real-time RT-PCR (qPCR), 2.5×10^5 hMBs were seeded on 60-mm dishes (AS ONE). The next day, the hGM was replaced with a differentiation medium (DM) for hMB (hDM) consisting of DMEM (Nacalai, Osaka, Japan), 2% horse serum (HyClone; Cytiva, Marlborough, MA, USA), and a mixture of 100 units/mL penicillin and 100 µg/mL streptomycin (P/S) (Nacalai), and PS-ODNs were treated at a final concentration of 30 µM for 48 h.

Murine myoblasts (mMBs) were isolated from the skeletal muscle of 4-week-old C57BL/6J mice (Clea Japan, Tokyo, Japan) as previously described [18]. Primary-cultured mMBs were maintained in a GM for mMB (mGM) consisting of Ham's F10 (Thermo Fisher Scientific, Waltham, MA, USA), 20% fetal bovine serum (FBS) (HyClone; Cytiva), 2 ng/mL recombinant human basic fibroblast growth factor (rh-bFGF) (Fujifilm Wako Chemicals, Osaka, Japan), and P/S. For the screening system, 1.0×10^4 mMBs/100 µL mGM/well were seeded on 96-well plates. The next day, the medium was replaced with a fresh mGM containing 10 µM PS-ODNs for 48 h.

Chicken myoblasts (chMBs) were isolated from the leg muscle of E10 embryos of broiler UK Chunkey chicken (National Federation of Agricultural Cooperative Associations, Tokyo, Japan) as previously described [9,19–21]. chMBs were maintained in a GM for chMB (chGM) consisting of RPMI1640 (Nacalai), 20% FBS, 1% non-essential amino acids (Fujifilm Wako Chemicals), 1% chicken embryo extract (US Biological, Salem, MA, USA), 2 ng/mL rh-bFGF, and P/S. For the screening system, 5.0×10^3 chMBs/100 µL chGM/well were seeded on 96-well plates. The next day, the medium was replaced with a fresh chGM containing 10 µM PS-ODNs for 48 h.

2.3. Immunocytochemistry

After 48 h of PS-ODN treatment, myoblasts were subjected to immunostaining for myosin heavy chain (MHC). The myoblasts were fixed with 2% paraformaldehyde, permeabilized with 0.2% Triton X-100, and immunostained with 0.5 µg/mL mouse monoclonal anti-MHC antibody (MF20; R&D Systems, Minneapolis, MN, USA). As a secondary antibody, 0.1 µg/mL of Alexa Fluor 488-conjugated donkey polyclonal anti-mouse IgG antibody

(Jackson ImmunoResearch, West Grove, PA, USA) was used. Cell nuclei were stained with DAPI (Nacalai). The screening system for analyzing MHC images has been described previously [7]. Briefly, fluorescence images were acquired automatically using CellInsight NXT (Thermo Fisher Scientific) and quantified using HCS Studio: Cellomics Scan software version 6.4.1 (Thermo Fisher Scientific) as follows: For hMBs and chMBs, MHC signal intensity was defined as the total MHC signal intensity divided by the total number of nuclei. For mMBs, the ratio of MHC⁺ cells was defined as the number of nuclei in the MHC⁺ cells divided by the number of nuclei. High-resolution MHC images (1280 × 960 pixels, 8 bit) were obtained using EVOS FL Auto microscope (AMAFD1000; Thermo Fisher Scientific) with ×10 objective magnification. Exposure time and bandpass filter (excitation/emission) were 100 ms and 470/510 nm for MHC and 15 ms and 357/447 nm for DAPI, respectively. The ratio of MHC⁺ cells was defined as the number of nuclei in all MHC⁺ cells divided by the total number of nuclei, and the fusion index was defined as the number of nuclei in multinucleated MHC⁺ myotubes divided by the total number of nuclei, which were calculated using ImageJ software version 1.52a (National Institutes of Health, Bethesda, MD, USA).

2.4. qPCR

After 24 h of PS-ODN treatment, the total RNA was isolated from hMBs using Nucleospin RNA Plus (Macherey-Nagel, Düren, Germany) and reverse transcribed using a ReverTra Ace qPCR RT Master Mix (TOYOBO, Osaka, Japan). qPCR was performed using a GoTaq qPCR Master Mix (Promega, Madison, WI, USA) with a StepOne Real-Time PCR System (Thermo Fisher Scientific). The amount of each transcript was normalized to that of the tyrosine 3-monooxygenase/tryptophan 5-monooxygenase activation protein zeta gene (YHHAZ). The primer sequences were described previously [7,11]. Results are expressed as fold-change.

2.5. Protein Precipitation and Western Blotting

Protein precipitation by PS-ODNs was performed as described previously [7]. The C2C12 murine myoblast cell line (DS Pharma Biomedical, Osaka, Japan) was maintained in DMEM supplemented with 10% FBS and P/S. A soluble whole-cell lysate of 1.0×10^7 C2C12 cells was prepared using 250 μ L of a lysis buffer consisting of 0.1 M Tris-HCl (pH 7.4), 75 mM NaCl, 1% Triton X-100, and a protease inhibitor cocktail (1 mM 4-(2-aminoethyl)benzenesulfonyl fluoride hydrochloride, 0.8 μ M aprotinin, 15 μ M E-64, 20 μ M leupeptin hemisulfate monohydrate, 50 μ M bestatin, and 10 μ M pepstatin A) (Nacalai). The PS-ODNs conjugated with biotin at the 5'-end (GeneDesign) were immobilized on streptavidin-coated magnetic beads (Magnosphere MS300/Streptavidin; JSR Life Sciences, Sunnyvale, CA, USA) according to the manufacturer's instructions. An amount of 100 μ g of lysates and 0.6 mg of iSN14 beads were mixed in 1 mL of a lysis buffer containing 1% NP-40 (Nacalai), and then gently rotated at 4 °C overnight to eliminate non-specific proteins absorbed on negative control PS-ODN or beads. After magnetic pull-down of iSN14 beads, the pre-treated supernatants were mixed with iSN04, iMyo01, or iMyo03 beads and rotated at 4 °C overnight. Proteins precipitated by PS-ODN beads were dissociated in a lysis buffer containing 1% NP-40, 10% glycerol, and 2% sodium dodecyl sulfate (SDS) at 95 °C for 5 min. The samples were subjected to 8% SDS-PAGE followed by Western blotting using an iBlot 2 Dry Blotting System (Thermo Fisher Scientific). The protein-transferred nitrocellulose membrane was blocked with 0.5% ECL Prime blocking agent (GE Healthcare, Chicago, IL, USA). An amount of 1.0 μ g/mL rabbit polyclonal anti-nucleolin antibody (ab22758; Abcam, Cambridge, UK) and 0.1 μ g/mL horseradish peroxidase (HRP)-conjugated goat anti-rabbit IgG antibody (Jackson ImmunoResearch) were used as primary and secondary antibodies, respectively. HRP activity was detected using ECL Prime reagents (GE Healthcare) and captured using ImageQuant LAS 500 (GE Healthcare).

2.6. Agarose Gel Electrophoresis

An amount of 0.8 nmol PS-ODNs and 0.8 nmol berberine hydrochloride (Nacalai) were mixed in 16 μL Ham's F10 containing 144.1 mM Na^+ , 0.6 mM Mg^{2+} , 5 mM K^+ , 0.3 mM Ca^{2+} , 1 μM Fe^{2+} , 1 μM Cu^{2+} , and 0.1 μM Zn^{2+} cations. The mixtures were placed at 4 $^{\circ}\text{C}$ overnight and then subjected to electrophoresis using a TAE-buffered 3% agarose gel with 0.5 $\mu\text{g}/\text{mL}$ ethidium bromide (EtBr). For monochromatic images, the gels were illuminated with 365 nm ultraviolet (UV) light and the images were captured using ImageQuant LAS 500 with a 560 nm emission bandpass filter (GE Healthcare). For colored images, the gels were illuminated by 302 nm UV light and the images were taken by a digital still camera without any filters to detect the 530 nm yellow emission from berberine and the 620 nm red emission from EtBr [7].

2.7. NMR

iMyo01-DNA was annealed by heating at 95 $^{\circ}\text{C}$ for 5 min followed by snap-cooling on ice. Annealed iMyo01 (final concentration of 0.7 mM) was dissolved in 20 mM sodium phosphate (pH 6.5) using a centrifuge concentrator (Vivaspin 3000 MWCO; Sartorius, Göttingen, Germany). For the K^+ condition, concentrated KCl was added to the sample to a final concentration of 50 mM. NMR spectra were measured using an AVANCE600 spectrometer (Bruker BioSpin, Billerica, MA, USA) at a probe temperature of 10 $^{\circ}\text{C}$. In this study, 1D imino proton spectra and 2D nuclear Overhauser effect spectroscopy (NOESY) spectra (mixing time of 150 ms) were recorded using the jump-and-return or 3-9-19 pulse schemes for water suppression.

2.8. Native PAGE

The conformation of iMyo01-DNA, iMyo01-CS, 12nt-Ctrl, and 12nt-Ctrl-CS was analyzed by 20% native PAGE with or without 5 mM KCl. A concentrated KCl solution was added to the gel and running TBE buffer. The gels were stained with SYBR Gold (Thermo Fisher Scientific).

2.9. Multicanonical Molecular Dynamics (McMD) Simulation

The two molecules of iMyo01-DNA in explicit solvent were simulated by the trivial-trajectory parallelization (TTP)-McMD method [7,16]. The simulation system (Supplementary Figure S1) contained two iMyo01-DNA molecules, 10,252 water molecules, 23 K^+ ions, and one Cl^- ion to be neutralized electrically. The initial structure of one iMyo01-DNA molecule was built as a DNA helix model by NAB in AmberTools 22 [22]. The other iMyo01-DNA was copied from the first and was separated by 10 \AA . The force field of amber OL15 [23] was applied for iMyo01-DNA. The TIP3P model [24] was used for water. The periodic boundary condition was used with a truncated octahedron box. The long-range interaction was calculated by particle-meshed Ewald with a 10 \AA cutoff.

The TTP-McMD [25] was conducted to sample the equilibrated conformations at 310 K. Before TTP-McMD, the volume of the system was equilibrated by MD simulation under the constant NPT condition of 1 bar. The energy range of the multicanonical ensemble covered from 270 K to 600 K. A total of 100 trajectories were used, and 14 iterative runs were performed to achieve a flat distribution along the energy range. The production run was conducted for 100 ns in each trajectory (total 10 μs). The snapshots were saved every 200 ps. A total of 50,000 snapshots were sampled, and the 988 conformations at 310 K were obtained as the 310 K canonical ensemble by the reweighting method.

The representative iMyo01-DNA structures were taken from the centroid of structural clustering using AmberTools22 [26], which was performed for the iMyo01-DNA molecules with the metrics of the root-mean square deviation of heavy atoms within iMyo01-DNA in the dimer state. A hydrogen bond analysis was performed using VMD tools version 1.9.4a53 [27]. The structure images were generated by UCSF Chimera [28].

2.10. Statistical Analysis

The results were presented as mean \pm standard error. Statistical comparisons were performed using multiple comparison tests with Dunnett's test following one-way analysis of variance. Statistical significance was set at $p < 0.05$.

3. Results

3.1. Designing and Screening of iMyo-ODNs

The established 18-base myoDN, iSN04, has a tandem telomeric repeat (TTA GGG TGA GGG) as the core sequence for its myogenetic activity. In particular, the G-stack consisting of the 13–15th GGG is an indispensable structure for iSN04 activity [7]. We designed eight non-telomeric PS-ODNs (iMyo-ODNs; iMyo01–iMyo08) with two G groups (GGG or GGGG) separated by a mini linker (T or TGA), thymines at the 5' end (TT or TTT), and adenines at the 3' end (AA or AAA) (Table 1). It has been speculated that iMyo-ODNs form a condensed conformation through interactions between 5'-terminal thymines and 3'-terminal adenines and have G-stacks within the structure, similar to that of iSN04.

To investigate the myogenetic activities of iMyo-ODNs, undifferentiated myoblasts were treated with PS-ODNs for 48 h and immunostained for MHC, a terminal differentiation marker of skeletal muscle. The signal intensities of MHC or the ratio of MHC⁺ cells were automatically quantified in an unbiased manner using the screening system (Figure 1). iSN04 was used as a positive control, and iSN14 and iSN45 served as negative controls. In hMBs, iMyo01 and iMyo03 significantly increased MHC signal intensities to the same extent as iSN04. Other iMyo-ODNs and negative controls did not induce myogenesis (Figure 1A). In mMBs, iMyo03 and iMyo04 markedly increased the ratio of MHC⁺ cells (Figure 1B). In chMBs, iMyo01–iMyo04 exhibited significant abilities to promote myogenic differentiation (Figure 1C). In all myoblasts, iMyo05–iMyo08 did not induce myogenesis, indicating that the latter GGGG, not GGG, is essential for iMyo-ODNs to function as myoDNs.

The effects of iMyo01 and iMyo03 on hMBs were further investigated by high-resolution imaging and qPCR (Figure 2). Immunostaining revealed that both iSN04 and iMyo01 significantly induced the differentiation of hMBs into MHC⁺ myocytes and multinucleated myotubes. iMyo03 also markedly accelerated myotube formation (Figure 2A). The mRNA levels of MyoD (*MYOD1*), a master regulator of myogenesis, were not altered by any of the PS-ODNs, but those of myogenin (*MYOG*), a myogenic transcription factor, were significantly increased by iMyo03 and were similarly induced by iSN04 and iMyo01. Transcriptions of myomaker (*MYMK*) and myomixer (*MYMX*), which are myogenin-regulated muscle-specific membrane proteins for myotube formation, were markedly upregulated by iSN04, iMyo01, and iMyo03 (Figure 2B). These results demonstrate that iMyo01 and iMyo03 as well as iSN04 promote the myogenic differentiation of hMBs.

3.2. iMyo01 and iMyo03 Bind to Nucleolin but Not to Berberine

Since iSN04 physically interacts with nucleolin to exert its myogenetic activity [7], iMyo01 and iMyo03 were tested for their ability to bind to nucleolin by precipitation assay. Biotin-conjugated PS-ODNs were immobilized on streptavidin beads. The soluble lysate of the C2C12 murine myoblast cell line was pre-pulled down with iSN14 beads to eliminate the absorption of non-specific proteins. After removing off-targets, the lysate was precipitated with iSN04, iMyo01, or iMyo03 beads. The precipitates were subjected to Western blotting to detect nucleolin. As shown in Figure 3A, nucleolin was precipitated by iMyo01 and iMyo03 as well as by iSN04.

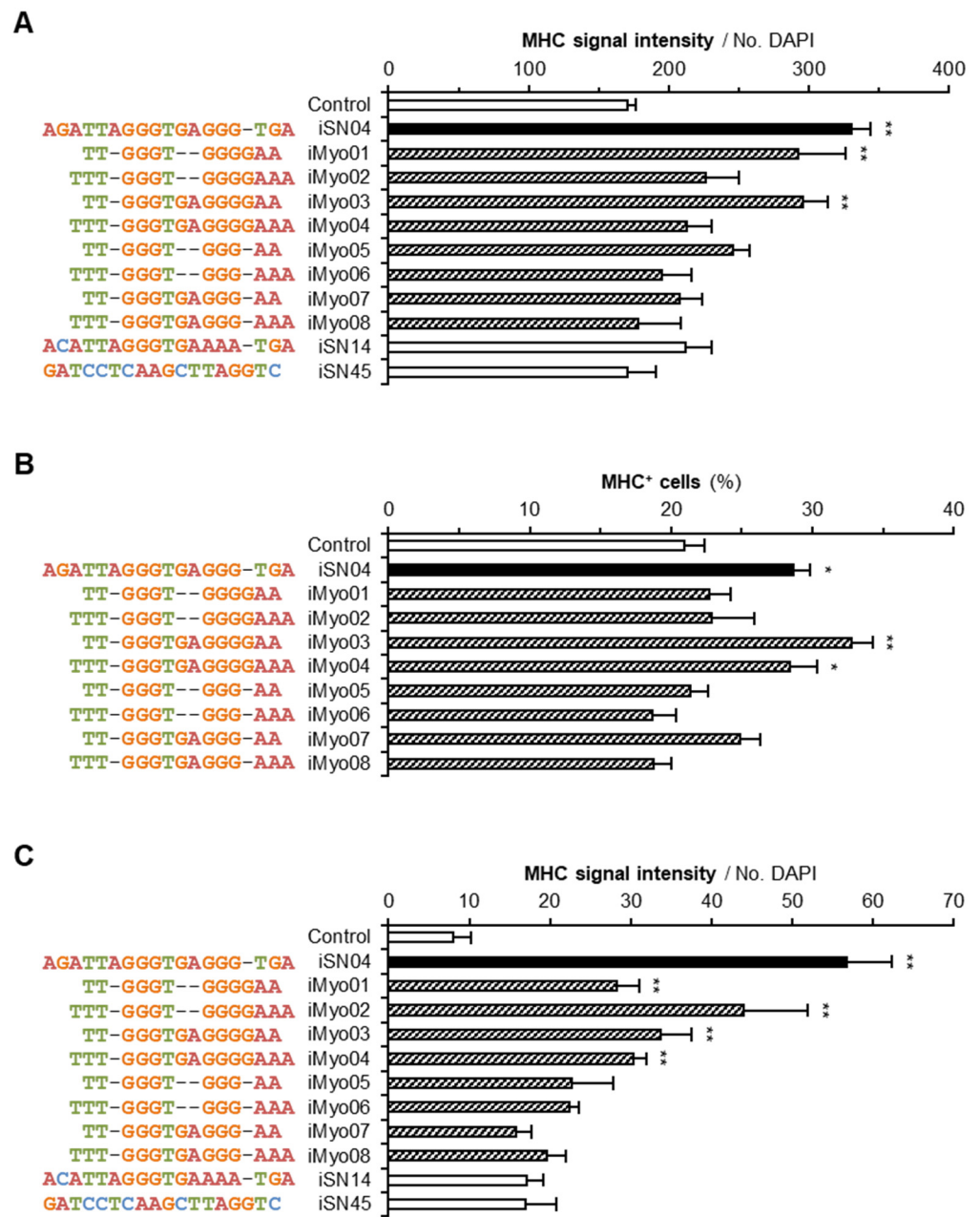


Figure 1. Myogenetic activities of iMyo-ODNs. (A) MHC signal intensities of hMBs treated with 30 μ M PS-ODNs in DM for 48 h. (B) The ratio of MHC⁺ cells within mMBs treated with 10 μ M PS-ODNs in mGM for 48 h. (C) MHC signal intensities of chMBs treated with 10 μ M PS-ODNs in chGM for 48 h. The results were presented as mean \pm standard error. * $p < 0.05$, ** $p < 0.01$ vs. control (Dunnett’s test). $n = 3$ technical replicates.

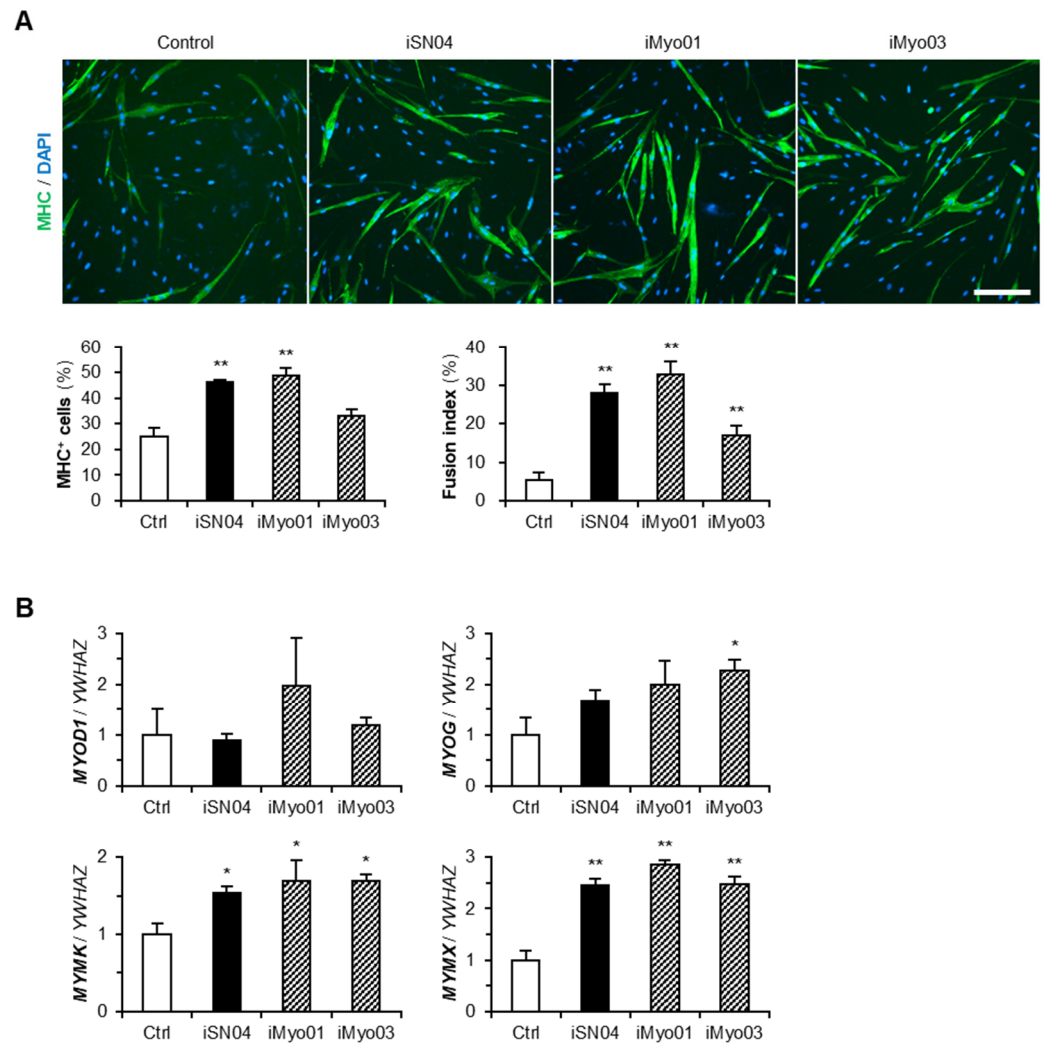


Figure 2. Effects of iMyo01 and iMyo03 on hMBs. **(A)** Representative fluorescence images of MHC staining of hMBs treated with 30 μ M PS-ODNs in DM for 48 h. Scale bar, 200 μ m. The ratio of MHC⁺ cells and multinucleated myotubes was quantified. The results were presented as mean \pm standard error. ** $p < 0.01$ vs. control (Dunnett's test). $n = 6$ –8 fields. **(B)** qPCR results of myogenic gene expression in hMBs treated with 30 μ M PS-ODNs in DM for 24 h. *YWHAZ*, tyrosine 3-monooxygenase/tryptophan 5-monooxygenase activation protein zeta gene as an internal control. The mean values of control hMB were set to 1.0. The results were presented as mean \pm standard error. * $p < 0.05$, ** $p < 0.01$ vs. control (Dunnett's test). $n = 3$ –4 independent experiments.

iSN04 also interacts with berberine via its G-stack (GGG at the 13–15th base) in the presence of Ca^{2+} or Mg^{2+} [7]. Berberine is an isoquinoline that binds to the G-quartet and stabilizes the G-quadruplex structure derived from telomeric sequences [29]. The iSN04–berberine complex shows higher myogenetic activity compared to iSN04 alone because berberine stabilizes the core G-stack within iSN04 [7]. To determine whether iMyo-ODNs form a complex with berberine, PS-ODNs and berberine were mixed in Ham's F10 and subjected to agarose gel electrophoresis. As shown in Figure 3B, the yellow emission from berberine (arrowhead) was detected at the same position as the red emission from iSN04 stained with EtBr (arrow), indicating the iSN04–berberine complex. However, all iMyo-ODNs, even the myogenetic iMyo01 and iMyo03, did not interact with berberine. This result suggests that the G-repeats of iMyo-ODNs form a different structure than the G-stack within iSN04. Since the myogenetic activities of iMyo01 and iMyo03 undoubtedly depend on their ability to bind to nucleolin, their conformations need to be determined directly.

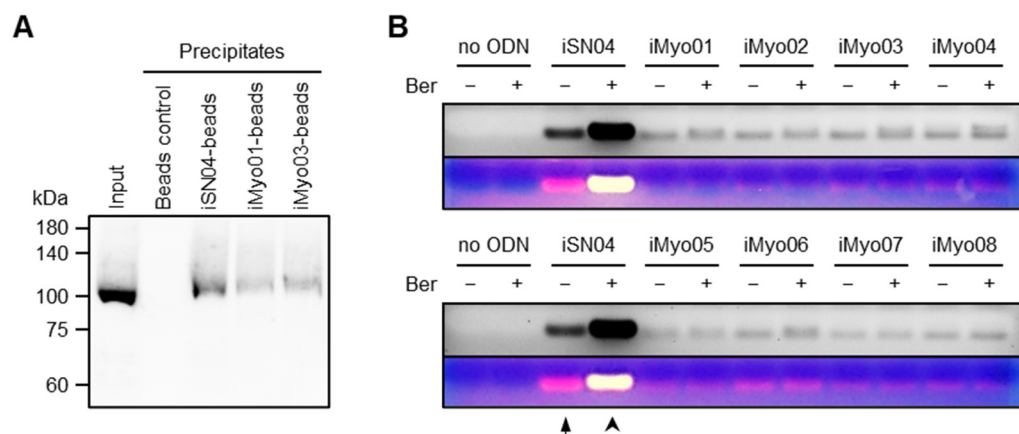


Figure 3. iMyo01 and iMyo03 bind to nucleolin but not to berberine. **(A)** Representative Western blotting image of nucleolin in the soluble whole-cell lysates of C2C12 cells precipitated by iSN04, iMyo01, or iMyo03. Beads control, streptavidin-coated beads without ODN. **(B)** Representative images of agarose gel electrophoresis of iSN04 and iMyo-ODNs mixed with berberine in Ham's F10. Ber, berberine. An arrow and an arrowhead indicate red and yellow emissions, respectively.

3.3. iMyo01 Forms a G-Quadruplex Structure

The imino proton NMR spectra of iMyo01-DNA were measured to characterize its structure (Figure 4A). In the absence of KCl, seven sharp (arrows) and four broad (arrowheads) signals were observed. After titration with 50 mM KCl, the NMR spectrum changed significantly, but seven sharp (arrows) and four broad (arrowheads) signals were observed, similar to those in the absence of KCl. The imino proton resonances between 10.5 and 12.5 ppm are characteristic for G-quadruplex formation [30], consistent with iMyo01 having no cytosine and therefore no G:C base pair. Since the G-quadruplex structure is stabilized by K^+ [31], it is considered that the KCl-induced shift of the imino proton spectrum of iMyo01-DNA represents the stabilization of its G-quadruplex by K^+ binding. To confirm G-quadruplex structure, the NOESY spectrum of iMyo01-DNA was measured (Figure 4B). The strong NOE signals between imino protons and NOE signals between H8 and imino protons strongly suggested that iMyo01-DNA forms the G-quadruplex (Figure 4B,C).

3.4. iMyo01 Forms a Homodimer in the Presence of K^+

The NMR results showed the G-quadruplex structure of iMyo01-DNA; however, the 12-base iMyo01 sequence with only two G-repeats is too short to form a G-quadruplex, which requires at least 16 bases including four G-repeats [32]. Therefore, it is assumed that iMyo01 forms a dimer to realize a G-quadruplex. The conformation of iMyo01-DNA was analyzed by native PAGE. As shown in Figure 5, iMyo01-CS (lane 6) was not stained with SYBR Gold due to its low number of purines (only three adenines), but other nucleotides were detected. iMyo01-DNA (lane 4) was observed in monomer mobility in the absence of KCl but was detected in dimer mobility in the presence of KCl, which is confirmed by the duplex of iMyo01-DNA and iMyo01-CS (lane 5). In contrast, no dimer mobility was observed for 12nt-Ctrl (lane 1), which never forms a G-quadruplex, even in the presence of KCl. The K^+ -dependent dimer formation strongly suggests that iMyo01-DNA forms a G-quadruplex structure in the presence of K^+ , in agreement with the results of the NMR.

Dimer formation of iMyo01-DNA was computationally simulated by McMD with the all-atom model. Using the simulated conformational ensemble, the distances between the centers of mass of the two iMyo01 molecules (d_{com}) were calculated. As shown in Supplementary Figure S2, their probability distributions showed that the dimer state ($d_{com} < 25 \text{ \AA}$) is more stable than the separated monomer state ($d_{com} \geq 25 \text{ \AA}$). The conformation at $d_{com} \approx 10 \text{ \AA}$ (arrow) had the highest probability, which was the most stable. Structural clustering of the dimer state represented the centroid structures of the top three clusters occupying 86.5% of all structures. Their d_{com} values were 6.0 (42.1%, Figure 6A),

11.4 (27.0%, Figure 6B), and 18.6 Å (17.5%, Figure 6C). Since the conformation at $d_{\text{com}} \approx 10$ Å showed the highest probability, those in the second cluster at $d_{\text{com}} = 11.4$ can be the stable dimer.

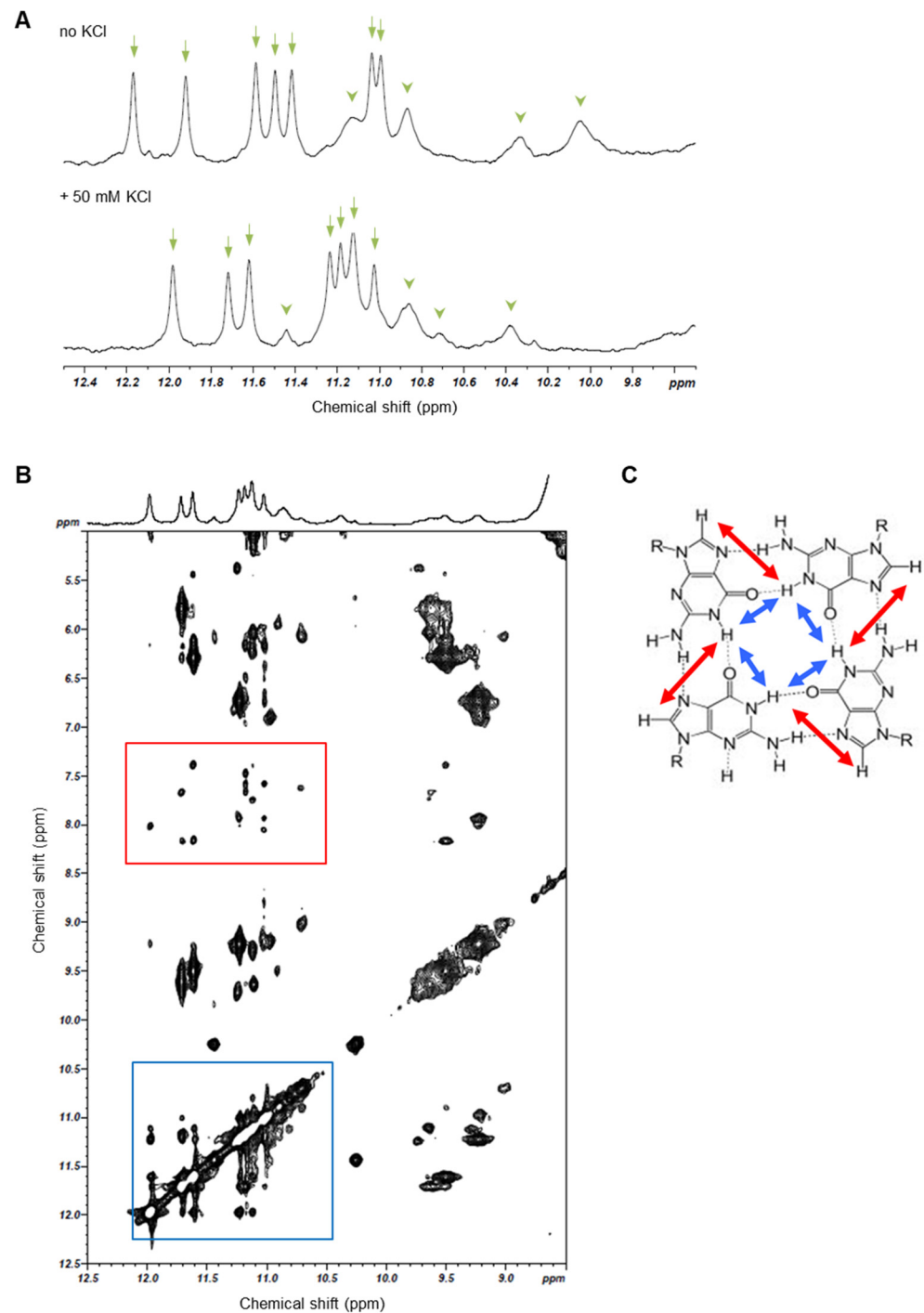


Figure 4. NMR analysis of iMyo01-DNA. (A) Comparison of 1D imino proton spectra of iMyo01-DNA in the absence of KCl and in the presence of 50 mM KCl. Arrows and arrowheads indicate seven sharp and four broad signals, respectively. (B) 2D NOESY spectrum (mixing time 150 ms). The NOE signals between imino protons (blue box) and the NOE signals between imino protons and H8 (red box). (C) Schematic representation of G-quartet and NOEs between imino protons (blue arrows) and between imino proton and H8 (red arrows).

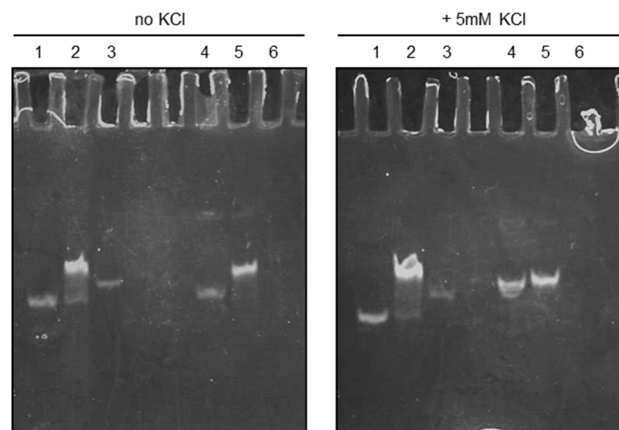


Figure 5. Native PAGE of iMyo01-DNA. Lane 1, 12nt-Ctrl; lane 2, duplex of 12nt-Ctrl and 12nt-Ctrl-CS; lane 3, 12nt-Ctrl-CS; lane 4, iMyo01-DNA; lane 5 duplex of iMyo01-DNA and iMyo01-CS; lane 6, iMyo01-CS, which was not stained with SYBR Gold due to its low purine content.

The analysis of the intra/intermolecular hydrogen bonds between the residues of iMyo01-DNA showed that the guanines form hydrogen bonds. The second cluster conformation indicated intermolecular hydrogen bonding between the G-repeats (Figure 6B), which may correspond to the G-quadruplex detected by NMR. On the other hand, the monomer state showed the intramolecular hydrogen bonds formed between G3-G5 and G7-G10 (Supplementary Figure S3), indicating that the monomer state had the stacking tandem guanines. Furthermore, the K^+ ions were found at the interface of iMyo01-DNA (Figure 6, purple spheres), which could reduce the electrostatic repulsion between them and thus contribute to the formation of the dimer. However, the G-stack in the dimer was slightly perturbed so that the simulated conformations did not have a fully coplanar arrangement of four guanines, suggesting that a more accurate force field of nucleic acids and solvents would be required to reproduce the complete G-tetrad.

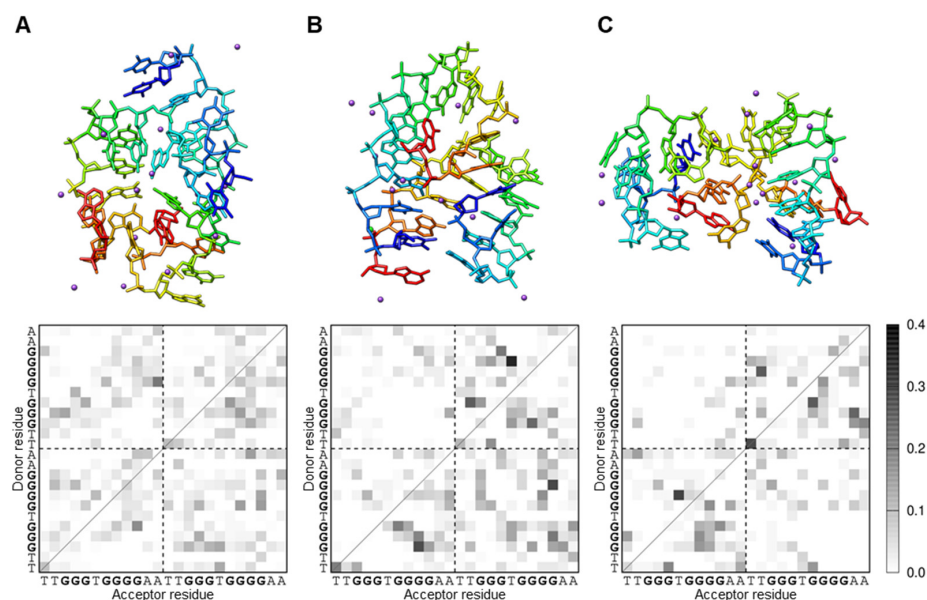


Figure 6. The representative iMyo01-DNA structures in the dimer state from McMD simulation. (A) The first cluster (42.1%; d_{com} , 6.0 Å). (B) The second cluster (27.0%; d_{com} , 11.4 Å). (C) The third cluster (17.5%; d_{com} , 18.6 Å). The clusters are shown as a rainbow-colored stick model from the 5' to the 3' end. The K^+ ions are shown as purple spheres. The hydrogen bond patterns in each cluster are plotted as a monochrome map. The gray scale indicates the probability of hydrogen bond formation between residues. The two iMyo01-DNA sequences are displayed sequentially on the axes.

4. Discussion

The present study successfully developed novel shorter myoDNs that promote myogenic differentiation. iMyo03 induced the differentiation of hMBs, mMBs, and chMBs as well as the established myoDN, iSN04, did. iMyo01 activated hMBs and chMBs, whereas iMyo02 and iMyo04 affected only chMBs. Such species-specificity of iMyo-ODNs may be due to the differences in nucleolin structures. Although myoDNs are considered to interact with four RNA-binding domains (RBD1-RBD4) of nucleolin [9], the amino acid sequences of the nucleolin RBDs are not completely conserved among animals (Table 2). A previous study has also reported that G-quadruplex anti-thrombin DNA aptamers (15-TBA, 31-TBA, and RA-36) individually exhibited different activities against various mammalian thrombins [33]. Clinically, aptamer cross-reactivity with the target ortholog in a patient can lead to side effects [34]. Our results suggest that modification of the existing aptamer can alter not only the affinity but also the cross-reactivity to the target molecule, which needs to be considered in aptamer design.

Table 2. Amino acid sequence identities of nucleolin RBDs.

RBD	Human vs. Mouse	Human vs. Chicken	Mouse vs. Chicken
RBD1	85.9%	56.4%	56.4%
RBD2	83.8%	69.3%	64.5%
RBD3	89.3%	71.1%	67.1%
RBD4	93.7%	88.2%	89.5%

In the previous study, nucleolin inhibition by iSN04 increased p53 protein levels [7] because nucleolin binds to p53 mRNA and represses its translation [35,36]. The present study confirmed that at least iMyo01 and iMyo03 physically interact with nucleolin. Thus, iMyo01 would increase p53 protein levels, resulting in the promotion of myogenesis because p53 cooperates with MyoD and the retinoblastoma protein to activate myogenic gene expression [37–39]. Furthermore, nucleolin has been reported to target several mRNAs, including Bcl-2, interleukin 2, and matrix metalloproteinase 9, in addition to p53, in cancer [40]. However, the role of nucleolin in myoblasts is poorly understood. Only one paper reported that miR-34b is involved in myoblast proliferation and differentiation via modulation of nucleolin protein levels [41]. To clarify the mechanism of action of iSN04 and iMyo01, the functions and targets of nucleolin in myoblasts need to be elucidated in further studies.

The 12-base iMyo01 is the shortest myoDN found and is two-thirds the length of the established 18-base iSN04. Both iMyo01 and iSN04 act as nucleolin-binding aptamers, and their lengths are much shorter than the average of known aptamers (51 bases) [42]. This is an advantage of our myoDNs as nucleic acid drugs. Because ODNs are chemically synthesized by sequential coupling of phosphoramidite monomers, longer ODNs have several issues related to purity, cost, and scalability for industrial mass production [43]. As biomolecules, longer ODNs have a greater chance of being phagocytized and cross-recognized [15], compromising drug efficacy and safety. Therefore, shortening aptamers while maintaining their activities is an important and beneficial challenge in the development of aptamers as nucleic acid drugs. In addition, myoDNs must be taken up into cells because their target protein, nucleolin, is located in the nuclei. However, iSN04 is incorporated into the cytoplasm without a carrier [7]; such gymnosis generally occurs with ODN treatments [14]. Since myoDNs need to cross plasma, endosomal, and nuclear membranes to reach nucleolin in the nucleus, the reduction in molecular weight will also contribute to their intracellular uptake.

On the other hand, the myogenetic activity of iMyo01 on hMBs was almost cell-physiologically equivalent to that of iSN04. The working doses of iSN04 and iMyo01 need to be carefully evaluated in further studies because iMyo01 acts as a homodimer. Although the nucleolin-binding ability of iMyo01 appeared to be lower than that of iSN04 in the

precipitation assay, this is probably due to the inability of iMyo01 immobilized on the beads to efficiently form homodimers.

Both experimental and computational results indicated that iMyo01-DNA forms a G-quadruplex structure by dimerization in the presence of K^+ . Unmodified DNA molecules were used for these cell-free structural analyses due to the absence of nucleases. The nuclease-resistant PS-ODNs were used for cellular experiments, but they are mixtures of enantiomers of phosphorothioates and are not suitable for conformational analysis. Although the formation and stabilization of tertiary structures of nucleic acids are possibly affected by nucleotide modifications, a UV thermodynamic analysis has shown that phosphorothioates do not have a significant effect on the stability of the G-quadruplex structure [44]. Therefore, the conformation of unmodified iMyo01-DNA confirmed by NMR and molecular simulation would essentially match that of PS-iMyo01. It is still difficult to selectively synthesize the designated enantiomer of PS-ODNs and is also hard to determine its structure experimentally. In silico calculations of configured enantiomers can be a powerful approach to overcome this problem and improve the productivity of aptamer design. The identification of iMyo01 in this study demonstrated that combined research technologies are useful for functional shortening of aptamers. It will hopefully contribute to the development of nucleic acid drugs.

For further applications of iMyo01, its efficacy and safety need to be evaluated in a variety of systems, including animal models. Myogenesis is a complex multi-step process from quiescent satellite cells to multinucleated giant myofibers [1]. Previous and current studies have shown that iSN04 and iMyo01 promote myogenic differentiation and myotube formation of myoblasts [7,9–12]. However, a decline in the myogenic capacity of myoblasts is one, but not the only, cause of age- and disease-related muscle loss [2–5]. Decreased numbers of satellite cells [45] and myofiber atrophy due to an imbalance between protein synthesis and degradation [46] are also major contributors to muscle wasting. Therefore, it is important to test myoDNs on satellite cells and myofibers to determine the therapeutic strategy. Except for our myoDNs, there are no aptamers that accelerate myogenesis, and there are no approved drugs for muscle wasting syndromes such as sarcopenia [47] and cachexia [48]. Anti-myostatin antibodies are expected to treat muscle loss, but one of the antibodies, LY2495655, did not improve muscle mass and function at least in pancreatic cancer [49]. For future success in reversing muscle loss, nucleic acid aptamers may be an indispensable drug modality. This study provides a candidate, iMyo01, and the wet and dry methodology for developing myogenic aptamers.

5. Conclusions

This study developed the 12-base short dimeric myoDN, iMyo01, which serves as an anti-nucleolin aptamer to promote myoblast differentiation as well as the well-known 18-base iSN04 can. iMyo01 dimerizes in the presence of K^+ to form a G-quadruplex structure, resulting in nucleolin-binding and myogenetic capabilities. This is a successful instance of shortening the aptamer while maintaining its bioactivity, providing useful insights for the development of aptamers as nucleic acid drugs.

6. Patents

K.U. and T.T. are the inventors of Japanese Patent No. 7386507 covering iMyo-induced myogenic differentiation.

Supplementary Materials: The following supporting information can be downloaded at <https://www.mdpi.com/article/10.3390/biotech13020011/s1>: Figure S1: The simulation system of the iMyo01-DNA dimer; Figure S2: The probability of the center-of-mass distances between the two iMyo01-DNA molecules; Figure S3: The representative iMyo01-DNA structure in the separated monomer state.

Author Contributions: Conceptualization, K.U. and T.T.; investigation, K.U., R.I., T.S. (Taiichi Sakamoto), Y.E., Y.N., S.S. and T.T.; resources, T.S. (Takeshi Shimosato) and H.K.; writing—original draft preparation, K.U., T.S. (Taiichi Sakamoto) and T.T.; funding acquisition, K.U., T.S. (Taiichi Sakamoto) and T.T. All authors have read and agreed to the published version of the manuscript.

Funding: This research was funded by the Japan Society for the Promotion of Science (19K05948 and 22K05554) to T.T.

Institutional Review Board Statement: The experimental procedures for the preparation of mMBs and chMBs were performed in accordance with the Regulations for Animal Experimentation of Shinshu University, and the animal protocol was approved by the Committee for Animal Experiments of Shinshu University (No. 280083; approved on 3 October 2017).

Informed Consent Statement: The hMBs used in this study are commercially available. Detailed information on the hMBs is described in a certificate analysis at https://bioscience.lonza.com/lonza_bs/CH/en/coa/search (accessed on 1 March 2024).

Data Availability Statement: The data presented in this study are available on request to the corresponding author.

Acknowledgments: The preprint has been posted on bioRxiv.

Conflicts of Interest: The authors declare no conflicts of interest.

References

1. Dumont, N.A.; Bentzinger, C.F.; Sincennes, M.C.; Rudnicki, M.A. Satellite cells and skeletal muscle regeneration. *Compr. Physiol.* **2015**, *5*, 1027–1059. [[PubMed](#)]
2. Brack, A.S.; Conboy, M.J.; Roy, S.; Lee, M.; Kuo, C.J.; Keller, C.; Rando, T.A. Increased Wnt signaling during aging alters muscle stem cell fate and increases fibrosis. *Science* **2007**, *317*, 807–810. [[CrossRef](#)] [[PubMed](#)]
3. Zhang, L.; Wang, X.H.; Wang, H.; Du, J.; Mitch, W.E. Satellite cell dysfunction and impaired IGF-1 signaling cause CKD-induced muscle atrophy. *J. Am. Soc. Nephrol.* **2010**, *21*, 419–427. [[CrossRef](#)] [[PubMed](#)]
4. Marchildon, F.; Lamarche, E.; Lala-Tabbert, N.; St-Louis, C.; Wiper-Bergeron, N. Expression of CCAAT/enhancer binding protein beta in muscle satellite cells inhibits myogenesis in cancer cachexia. *PLoS ONE* **2015**, *10*, e0145583. [[CrossRef](#)] [[PubMed](#)]
5. Henriksen, T.I.; Davidsen, P.K.; Pedersen, M.; Schultz, H.S.; Hansen, N.S.; Larsen, T.J.; Vaag, A.; Pedersen, B.K.; Nielsen, S.; Scheele, C. Dysregulation of a novel miR-23b/27b-p53 axis impairs muscle stem cell differentiation of humans with type 2 diabetes. *Mol. Metab.* **2017**, *6*, 770–779. [[CrossRef](#)] [[PubMed](#)]
6. Wang, T.; Chen, C.; Larcher, L.M.; Barrero, R.A.; Veedu, R.N. Three decades of nucleic acid aptamer technologies: Lessons learned, progress and opportunities on aptamer development. *Biotechnol. Adv.* **2019**, *37*, 28–50. [[CrossRef](#)] [[PubMed](#)]
7. Shinji, S.; Umezawa, K.; Nihashi, Y.; Nakamura, S.; Shimosato, T.; Takaya, T. Identification of the myogenetic oligodeoxynucleotides (myoDNs) that promote differentiation of skeletal muscle myoblasts by targeting nucleolin. *Front. Cell Dev. Biol.* **2021**, *8*, 616706. [[CrossRef](#)] [[PubMed](#)]
8. Nohira, N.; Shinji, S.; Nakamura, S.; Nihashi, Y.; Shimosato, T.; Takaya, T. Myogenetic oligodeoxynucleotides as anti-nucleolin aptamers inhibit the growth of embryonal rhabdomyosarcoma cells. *Biomedicines* **2022**, *10*, 2691. [[CrossRef](#)] [[PubMed](#)]
9. Nihashi, Y.; Shinji, S.; Umezawa, K.; Shimosato, T.; Ono, T.; Kagami, H.; Ono, T.; Kagami, H.; Takaya, T. Myogenetic oligodeoxynucleotide complexed with berberine promotes differentiation of chicken myoblasts. *Anim. Sci. J.* **2021**, *92*, e13597. [[CrossRef](#)]
10. Nakamura, S.; Yonekura, S.; Shimosato, T.; Takaya, T. Myogenetic oligodeoxynucleotide (myoDN) recovers the differentiation of skeletal muscle myoblasts deteriorated by diabetes mellitus. *Front. Physiol.* **2021**, *12*, 679152. [[CrossRef](#)]
11. Nihashi, Y.; Yamamoto, M.; Shimosato, T.; Takaya, T. Myogenetic oligodeoxynucleotide restores differentiation and reverses inflammation of myoblasts aggravated by cancer-conditioned medium. *Muscles* **2022**, *1*, 111–120. [[CrossRef](#)]
12. Yamamoto, M.; Miyoshi, M.; Morioka, K.; Mitani, T.; Takaya, T. Anti-nucleolin aptamer, iSN04, inhibits the inflammatory responses in C2C12 myoblasts by modulating the β -catenin/NF- κ B signaling pathway. *Biochem. Biophys. Res. Commun.* **2023**, *664*, 1–8. [[CrossRef](#)] [[PubMed](#)]
13. Ishioka, M.; Nihashi, Y.; Sunagawa, Y.; Umezawa, K.; Shimosato, T.; Kagami, H.; Morimoto, T.; Takaya, T. Myogenetic oligodeoxynucleotide induces myocardial differentiation of murine pluripotent stem cells. *Int. J. Mol. Sci.* **2023**, *24*, 14380. [[CrossRef](#)] [[PubMed](#)]
14. Juliano, R.L. Intracellular trafficking and endosomal release of oligonucleotides: What we know and what we don't. *Nucleic Acid Ther.* **2018**, *28*, 166–177. [[CrossRef](#)] [[PubMed](#)]
15. Pandey, A.K.; Rajput, Y.S.; Singh, D.; Sharma, R. Prediction of shorter oligonucleotide sequences recognizing aflatoxin M1. *Biotechnol. Appl. Biochem.* **2018**, *65*, 397–406. [[CrossRef](#)] [[PubMed](#)]
16. Nihashi, Y.; Miyoshi, M.; Umezawa, K.; Shimosato, T.; Takaya, T. Identification of a novel osteogenetic oligodeoxynucleotide (osteoDN) that promotes osteoblast differentiation in a TLR9-independent manner. *Nanomaterials* **2022**, *12*, 1680. [[CrossRef](#)] [[PubMed](#)]

17. Straarup, E.M.; Fisker, N.; Hedtjarn, M.; Lindholm, M.W.; Rosenbohm, C.; Aarup, V.; Hansen, H.F.; Orum, H.; Hansen, J.B.; Koch, T. Short locked nucleic acid antisense oligonucleotides potently reduce apolipoprotein B mRNA and serum cholesterol in mice and non-human primates. *Nucleic Acids Res.* **2010**, *38*, 7100–7111. [[CrossRef](#)]
18. Takaya, T.; Nihashi, Y.; Kojima, S.; Ono, T.; Kagami, H. Autonomous xenogenic cell fusion of murine and chick skeletal muscle myoblasts. *Anim. Sci. J.* **2017**, *88*, 1880–1885. [[CrossRef](#)]
19. Nihashi, Y.; Ono, T.; Kagami, H.; Takaya, T. Toll-like receptor ligand-dependent inflammatory responses in chick skeletal muscle myoblasts. *Dev. Comp. Immunol.* **2019**, *91*, 115–122. [[CrossRef](#)]
20. Nihashi, Y.; Umezawa, K.; Shinji, S.; Hamaguchi, Y.; Kobayashi, H.; Kono, T.; Ono, T.; Kagami, H.; Takaya, T. Distinct cell proliferation, myogenic differentiation, and gene expression in skeletal muscle myoblasts of layer and broiler chickens. *Sci. Rep.* **2019**, *9*, 16527. [[CrossRef](#)]
21. Takaya, T.; Nihashi, Y.; Ono, T.; Kagami, H. Transcription of endogenous retrovirus group K members and their neighboring genes in chicken skeletal muscle myoblasts. *J. Poult. Sci.* **2021**, *58*, 79–87. [[CrossRef](#)] [[PubMed](#)]
22. Macke, T.J.; Case, D.A. Modeling unusual nucleic acid structures. In *Molecular Modeling of Nucleic Acids*; Leontis, N.B., SantaLucia, J., Eds.; American Chemical Society: Washington, DC, USA, 1998; pp. 379–393.
23. Galindo-Murillo, R.; Robertson, J.C.; Zgarbova, M.; Sponer, J.; Otyepka, M.; Jurecka, P.; Cheatham, T.E., 3rd. Assessing the current state of Amber force field modifications for DNA. *J. Chem. Theory. Comput.* **2016**, *12*, 4114–4127. [[CrossRef](#)] [[PubMed](#)]
24. Jorgensen, W.L.; Chandrasekhar, J.; Madura, J.D.; Impey, R.W.; Klein, M.L. Comparison of simple potential functions for simulating liquid water. *J. Chem. Phys.* **1983**, *79*, 926–935. [[CrossRef](#)]
25. Ikebe, J.; Umezawa, K.; Kamiya, N.; Sugihara, T.; Yonezawa, Y.; Takano, Y.; Nakamura, H.; Higo, J. Theory for trivial trajectory parallelization of multicanonical molecular dynamics and application to a polypeptide in water. *J. Comput. Chem.* **2011**, *32*, 1286–1297. [[CrossRef](#)] [[PubMed](#)]
26. Case, D.A.; Aktulga, H.M.; Belfon, K.; Ben-Shalom, I.Y.; Berryman, J.T.; Brozell, S.R.; Cerutti, D.S.; Cheatham, T.E., 3rd; Cisneros, G.A.; Cruzeiro, V.W.D.; et al. *Amber 2023*; University of California: San Francisco, CA, USA, 2023.
27. Humphrey, W.; Dalke, A.; Schulten, K. VMD: Visual molecular dynamics. *J. Mol. Graph.* **1996**, *14*, 33–38. [[CrossRef](#)] [[PubMed](#)]
28. Pettersen, E.F.; Goddard, T.D.; Huang, C.C.; Couch, G.S.; Greenblatt, D.M.; Meng, E.C.; Ferrin, T.E. UCSF Chimera—A visualization system for exploratory research and analysis. *J. Comput. Chem.* **2004**, *25*, 1605–1612. [[CrossRef](#)] [[PubMed](#)]
29. Bazzicalupi, C.; Ferraroni, M.; Billa, A.R.; Scheggi, F.; Gratteri, P. The crystal structure of human telomeric DNA complexed with berberine: An interesting case of stacked ligand to G-tetrad ratio higher than 1:1. *Nucleic Acids Res.* **2013**, *41*, 632–638. [[CrossRef](#)] [[PubMed](#)]
30. Fukunaga, J.; Nomura, Y.; Tanaka, Y.; Torigoe, H.; Nakamura, Y.; Sakamoto, T.; Kozu, T. A G-quadruplex-forming RNA aptamer binds to the MTG8 TAFH domain and dissociates the leukemic AML1-MTG8 fusion protein from DNA. *FEBS Lett.* **2020**, *594*, 3477–3489. [[CrossRef](#)] [[PubMed](#)]
31. Awadasseid, A.; Ma, X.; Wu, Y.; Zhang, W. G-quadruplex stabilization via small-molecules as a potential anti-cancer strategy. *Biomed. Pharmacother.* **2021**, *139*, 111550. [[CrossRef](#)] [[PubMed](#)]
32. Guedin, A.; Gros, J.; Alberti, P.; Mergny, J.L. How long is too long? Effects of loop size on G-quadruplex stability. *Nucleic Acids Res.* **2010**, *38*, 7858–7868. [[CrossRef](#)]
33. Zavyalova, E.; Golovin, A.; Timoshenko, T.; Babiy, A.; Pavlova, G.; Kopylov, A. DNA aptamers for human thrombin with high anticoagulant activity demonstrate target- and species-specificity. *Curr. Med. Chem.* **2012**, *19*, 5232–5237. [[CrossRef](#)] [[PubMed](#)]
34. Lakhin, A.V.; Tarantul, V.Z.; Gening, L.V. Aptamers: Problems, solutions and prospects. *Acta Naturae* **2013**, *5*, 34–43. [[CrossRef](#)] [[PubMed](#)]
35. Takagi, M.; Absalon, M.J.; McLure, K.G.; Kastan, M.B. Regulation of p53 translation and induction after DNA damage by ribosomal protein L26 and nucleolin. *Cell* **2005**, *123*, 49–63. [[CrossRef](#)]
36. Chen, J.; Guo, K.; Kastan, M.B. Interactions of nucleolin and ribosomal protein L26 (RPL26) in translational control of human p53 mRNA. *J. Biol. Chem.* **2012**, *287*, 16467–16476. [[CrossRef](#)]
37. Cerone, M.A.; Marchetti, A.; Bossi, G.; Blandino, G.; Sacchi, A.; Soddu, S. p53 is involved in the differentiation but not in the differentiation-associated apoptosis of myoblasts. *Cell Death Differ.* **2000**, *7*, 506–508. [[CrossRef](#)]
38. Porrello, A.; Cerone, M.A.; Coen, S.; Gurtner, A.; Fontemaggi, G.; Cimino, L.; Piaggio, G.; Sacchi, A.; Soddu, S. p53 regulates myogenesis by triggering the differentiation activity of pRb. *J. Cell Biol.* **2000**, *151*, 1295–1304. [[CrossRef](#)]
39. Harford, T.J.; Kliment, G.; Shukla, G.C.; Weyman, C.M. The muscle regulatory transcription factor MyoD participates with p53 to directly increase the expression of the pro-apoptotic Bcl2 family member PUMA. *Apoptosis* **2017**, *22*, 1532–1542. [[CrossRef](#)]
40. Abdelmohsen, K.; Gorospe, M. RNA-binding protein nucleolin in disease. *RNA Biol.* **2012**, *9*, 799–808. [[CrossRef](#)]
41. Tang, Z.; Qiu, H.; Luo, L.; Liu, N.; Zhong, J.; Kang, K.; Gou, D. miR-34b modulates skeletal muscle cell proliferation and differentiation. *J. Cell. Biol.* **2017**, *118*, 4285–4295. [[CrossRef](#)] [[PubMed](#)]
42. Lee, G.; Jang, G.H.; Kang, H.Y.; Song, G. Predicting aptamer sequences that interact with target proteins using an aptamer-protein interaction classifier and a Monte Carlo tree search approach. *PLoS ONE* **2021**, *16*, e0253760. [[CrossRef](#)]
43. Molina, A.G.; Sanghvi, Y.S. Liquid-phase oligonucleotide synthesis: Past, present, and future predictions. *Curr. Protoc. Nucleic Acid Chem.* **2019**, *77*, e82. [[CrossRef](#)] [[PubMed](#)]
44. Sacca, B.; Lacroix, L.; Mergny, J.L. The effect of chemical modifications on the thermal stability of different G-quadruplex-forming oligonucleotides. *Nucleic Acids Res.* **2005**, *33*, 1182–1192. [[CrossRef](#)] [[PubMed](#)]

45. Hwang, A.B.; Brack, A.S. Muscle stem cells and aging. *Curr. Top. Dev. Biol.* **2018**, *126*, 299–322. [[PubMed](#)]
46. McCormick, R.; Vasilaki, A. Age-related changes in skeletal muscle: Changes to life-style as a therapy. *Biogerontology* **2018**, *19*, 519–536. [[CrossRef](#)] [[PubMed](#)]
47. Rolland, Y.; Dray, C.; Vellas, B.; Barreto, P.S. Current and investigational medications for the treatment of sarcopenia. *Metabolism* **2023**, *149*, 155597. [[CrossRef](#)] [[PubMed](#)]
48. Domaniku, A.; Bilgic, S.N.; Kir, S. Muscle wasting: Emerging pathways and potential drug targets. *Trends Pharmacol. Sci.* **2023**, *44*, 705–718. [[CrossRef](#)]
49. Golan, T.; Geva, R.; Richards, D.; Madhusudan, S.; Lin, B.K.; Wang, H.T.; Walgren, R.A.; Stemmer, S.M. LY2495655, an antimyostatin antibody, in pancreatic cancer: A randomized, phase 2 trial. *J. Cachexia Sarcopenia Muscle* **2018**, *9*, 871–879. [[CrossRef](#)]

Disclaimer/Publisher’s Note: The statements, opinions and data contained in all publications are solely those of the individual author(s) and contributor(s) and not of MDPI and/or the editor(s). MDPI and/or the editor(s) disclaim responsibility for any injury to people or property resulting from any ideas, methods, instructions or products referred to in the content.